INSTITUTE OF PHYSICS PUBLISHING SMART MATERIALS AND STRUCTURES
Smart Mater. Struct. **13** (2004) 791–799 PII: S0964-1726(04)78863-1

The use of polyvinylidene fluoride films as sensors for the experimental modal analysis of structures

Rong-Liang Chen[1] **and Bor-Tsuen Wang**[2,3]

[1] Center for Measurement Standards, Industrial Technology Research Institute, Hsinchu 30042, Taiwan
[2] Department of Mechanical Engineering, National Pingtung University of Science and Technology, Pingtung 91207, Taiwan

E-mail: wangbt@mail.npust.edu.tw

Received 20 August 2002, in final form 20 February 2004
Published 1 June 2004
Online at stacks.iop.org/SMS/13/791
doi:10.1088/0964-1726/13/4/017

Abstract
This work presents the use of a rectangular shape of PVDF (polyvinylidene fluoride) film adhered on the surface of a cantilever beam and a simply supported plate as the sensor, while the impact hammer is applied as the actuator for the structural modal testing. This work first formulates the frequency response function (FRF) based on the hammer excitation and PVDF sensing. The hammer actuator eigenfunction and the PVDF sensor eigenfunction can be identified as the displacement mode shape and the mode shape of the slope difference between the PVDF edges, respectively. A dual-channel FFT analyzer is used to perform the experiments. A row of the FRF matrix can be obtained when the PVDF sensor is roving with the hammer actuator fixed. The MDOF curve-fitting algorithm is used to extract the modal parameters, including natural frequencies, mode shapes and modal damping ratios of the structures. The frequency response functions are shown to agree reasonably well between theoretical and experimental results. Results also show that modal parameters can be properly obtained and physically interpreted with theoretical solutions. This work, therefore, demonstrates the feasibility of using the PVDF sensor in conjunction with the hammer for structural modal testing and can also be extended to other structures.

(Some figures in this article are in colour only in the electronic version)

Nomenclature

A_v	the area of PVDF sensor
b_b	beam width
e_{31}, e_{32}	piezoelectric field intensity constants
E_b	Young's modulus of beam
E_p	Young's modulus of plate
F_j	the jth impact force amplitude
I_b	cross sectional moment of inertia of the beam
L_b	beam length
l_v	the width PVDF sensor
l_{vx}	the width of the PVDF film
l_{vy}	the length of the PVDF film
L_x	the width of the plate
L_y	the length of the plate
t_b	beam thickness
t_p	plate thickness
t_v	thickness of the PVDF film
V_{v_i}	the ith PVDF voltage
x_{f_j}, y_{f_j}	the location of the jth hammer actuator in x- and y-coordinates

[3] Author to whom any correspondence should be addressed.

x_{v_i}, y_{v_i} the PVDF sensor central location in x- and y-coordinates
$x_{v_{1i}}$, $x_{v_{2i}}$ the location of the ith PVDF sensor in x-coordinates
$y_{v_{1i}}$, $y_{v_{2i}}$ the location of the ith PVDF sensor in y-coordinates
α_m, α_n the characteristic values
$\alpha_{v_i f_j}$ the FRF between the voltage of the ith PVDF sensor and the force amplitude of the jth hammer actuator
ω excitation frequency
ω_{mn} the mnth natural frequency of the plate
ω_n the nth natural frequency of the beam
ν_p Poisson's ratio of the plate
ρ_b beam density
ρ_p plate density
ε the permittivity of the PVDF sensor
ξ_{mn} the mnth modal damping ratio of the plate
ξ_n the nth modal damping ratio of the beam
$\phi_{mn}(x, y)$ the mnth displacement mode shape of the plate
$\phi^f_{mn,j}$ the mnth hammer mode shape function of the plate at the jth location of the hammer actuator
$\phi^v_{mn,i}$ the mnth PVDF mode shape function of the plate at the ith location of the PVDF sensor
ϕ_n the nth displacement mode shape of the beam
$\phi^v_{n,i}$ the nth PVDF mode shape function of the beam at the ith location of the PVDF sensor
$\phi^f_{n,j}$ the nth hammer mode shape function of the beam at the jth location of the hammer actuator

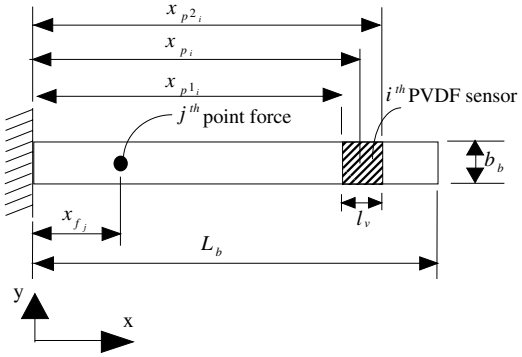

Figure 1. The arrangement of coordinates on the cantilever beam.

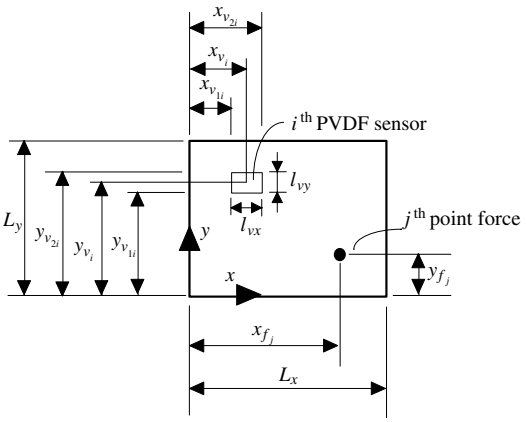

Figure 2. The arrangement of coordinates on the plate.

1. Introduction

Piezoelectric materials have attracted much research such as on active structural vibration and acoustic control. The rectangular shape of a PVDF film was introduced by Hubbard (1987) for the application to vibration control of beam structures as the sensor. Lee and Moon (1990) and Collins *et al* (1992) developed a special shape of PVDF film to sense the specific vibration modal response as known modal sensors. Galea *et al* (1993) applied the PVDF film as sensor to structural fault diagnosis and health monitoring. Collet and Jezequel (1994) and Tanaka *et al* (1996) utilized similar configurations of PVDF film as modal filters for vibration control.

The conventional approach of experimental modal analysis is to determine the modal properties. The point type of actuator such as the shaker or impact hammer is generally used, and the accelerometer is used as the sensor (Han and McConnell 1991, Hu and McConnell 1993, Worden *et al* 1994). The adoption of piezoceramic transducers for structural modal testing has also drawn attention. Sun *et al* (1994) derived the frequency response function (FRF) through electric admittance of piezoceramic transducers to obtain the dynamic parameters of beam structures. However, they did not physically interpret those dynamic parameters. Norwood (1995) successfully applied both the impact hammer and PVDF film, respectively, as actuation sources for the modal testing of cylindrical shell structures. Wang (1996) derived the frequency response functions between the traditional and piezoelectric transducers for a simply supported beam. He introduced the feasibility of the use of piezoelectric transducers for structural modal testing.

Wang (1998) generalized the formulation of frequency response functions (FRFs) for continuous structure systems subject to various forms of actuators and sensors. The actuator and sensor eigenfunctions (mode shapes) were respectively identified and physically interpreted according to the testing procedures, either roving the actuator or the sensor. Wang's work provided the theoretical base for the application of smart materials, such as PZT actuators and PVDF sensors, to smart structural testing. Previous work (Wang and Wang 1997) has theoretically demonstrated the feasibility of using piezoceramic transducers for cantilever beam modal testing. An array of finite-length PVDF films was assumed to be equally spaced and distributed over the beam acting as sensors, while a fixed pure-bending PZT actuator served as actuation force. They have performed synthetic modal analysis to extract modal parameters of the beam by using piezoceramic transducers. This paper will experimentally validate the use of PVDF films as sensors and a hammer as the actuator for structural modal testing of a cantilever beam and a simply supported plate. The system FRFs between the hammer actuator and PVDF sensor are measured. The modal parameters, including natural frequencies, mode shapes and damping ratios, can be extracted. In particular, the PVDF sensor mode shape function is characterized as the slope-difference mode shapes.

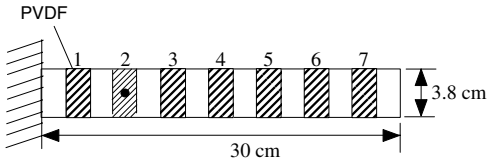

(a) division and number

(b) substance picture

Figure 3. Illustration of cantilever beam.

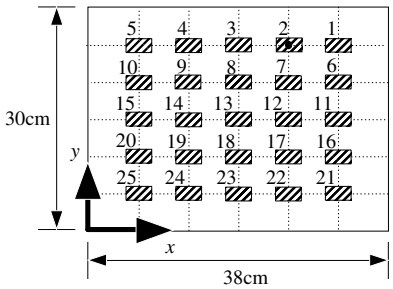

(a) division and number

(b) substance picture

Figure 4. Illustration of simply supported plate.

2. Theoretical analysis

2.1. Theoretical analysis of cantilever beam

A brief review of the theoretical analysis for the cantilever beam is summarized as follows (Wang and Wang 1997). From the free vibration analysis, the natural frequencies and the corresponding displacement mode shape functions can be identified as follows (Meirovich 1986):

$$\omega_n = (\alpha_n L_\mathrm{b})^2 \sqrt{\frac{E_\mathrm{b} I_\mathrm{b}}{\rho_\mathrm{b} b_\mathrm{b} t_\mathrm{b} L_\mathrm{b}^4}} = \alpha_n^2 \sqrt{\frac{E_\mathrm{b} I_\mathrm{b}}{\rho_\mathrm{b} b_\mathrm{b} t_\mathrm{b}}} \tag{1}$$

$$\phi_n(x) = \cosh \alpha_n x - \cos \alpha_n x - \sigma_n(\sinh \alpha_n x - \sin \alpha_n x) \tag{2}$$

where

$$\sigma_n = \frac{\sinh \alpha_n L_\mathrm{b} - \sin \alpha_n L_\mathrm{b}}{\cosh \alpha_n L_\mathrm{b} + \cos \alpha_n L_\mathrm{b}}. \tag{3}$$

The eigenvalue (α_n, $n = 1, 2, \ldots$) can be expressed as follows (Blevins 1979):

$$\begin{aligned} \alpha_1 L_\mathrm{b} &= 1.875\,104 \\ \alpha_2 L_\mathrm{b} &= 4.694\,091 \\ \alpha_3 L_\mathrm{b} &= 7.854\,757 \\ &\vdots \end{aligned} \tag{4}$$

A strip of PVDF film can also be applied as the sensing device as shown in figure 1. The FRF between the measured voltage of the ith PVDF sensor, V_{v_i}, and the force amplitude applied by the hammer actuator, F_j, can be obtained as follows (Wang 1998):

$$\alpha_{v_i f_j}(\omega) = \frac{V_{v_i}}{F_j} = \sum_{n=1}^{\infty} \frac{\phi_{n,i}^v \phi_{n,j}^f}{(\omega_n^2 - \omega^2) + \mathrm{i}(2\xi_n \omega_n \omega)} \tag{5}$$

where

Table 1. Physical properties of cantilever beam.

Material	Steel
Length, L_b (m)	0.3
Width, b_b (m)	0.04
Thickness, t_b (m)	0.002
Density, ρ_b (kg m^{-3})	7870
Young's modulus, E_b (N m^{-2})	207×10^9

Table 2. Physical properties of PVDF sensor.

Type		DT1-028K
Beam	Length, l_v (mm)	20
Plate	Length, l_{vx} (mm)	38
	Width, l_{vy} (mm)	19
	Thickness, t_v (m)	28×10^{-6}
	Young's modulus, E_v (N m^{-2})	6.3×10^{10}
	Density, ρ_v (kg m^{-3})	1800
	Poisson ratio, ν_v	0.33
	Piezoelectric field intensity constant, $e_{31} = e_{32}$ (m V^{-1})	54×10^{-3}
	Permittivity, ε (F m^{-1})	106×10^{-12}

$$\phi_{n,j}^f = \frac{1}{\sqrt{\rho_\mathrm{b} b_\mathrm{b} t_\mathrm{b} L_\mathrm{b}}} \phi_n(x_{f_j}) \tag{6}$$

$$\phi_{n,i}^v = \frac{1}{\sqrt{\rho_\mathrm{b} b_\mathrm{b} t_\mathrm{b} L_\mathrm{b}}} k_v [\phi_n'(x_{v_{2i}}) - \phi_n'(x_{v_{1i}})] \tag{7}$$

$$k_v = \frac{t_v}{\varepsilon A_v} \frac{t_\mathrm{b} + t_v}{2} l_v e_{31}. \tag{8}$$

$\phi_{n,i}^v$ and $\phi_{n,j}^f$ represent the values of the nth PVDF sensor and hammer actuator mode shape functions at the ith and jth location of the PVDF sensor and hammer actuator, respectively. The PVDF mode shape functions are

Table 3. Comparison of the natural frequencies of the cantilever beam between theoretical and experimental results.

Natural frequency	Theoretical (Hz)	Experimental (Hz)		Error percentage (%)	
		Acc./hammer	PVDF/hammer	Acc./hammer	PVDF/hammer
f_1	18.41	18.01	17.32	−2.18	−5.93
f_2	115.38	113.58	109.52	−1.56	−5.08
f_3	323.06	318.00	306.00	−1.59	−5.28
f_4	633.06	624.39	598.62	−1.83	−5.44

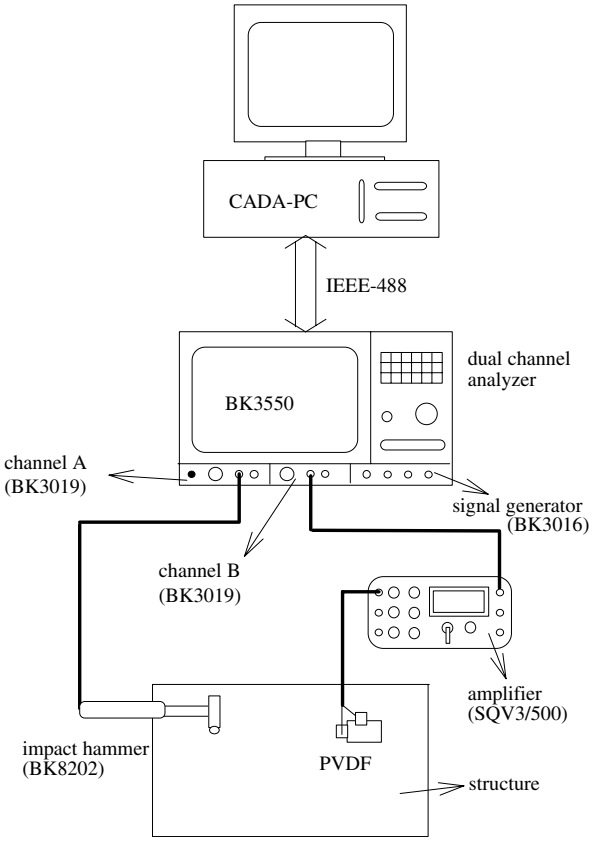

Figure 5. Experimental equipment layout.

Table 4. The experimental modal damping of the cantilever beam.

Mode	Damping ratio (%)
ξ_1	4.95
ξ_2	0.97
ξ_3	0.32
ξ_4	0.24

proportional to the mode shape of the slope difference between the two edges of PVDF film and can be shown to be the mirror image of displacement mode shapes against the clamped end (Wang and Wang 1997).

2.2. Theoretical analysis of simply supported plate

The thin plate theory is adopted, and the natural frequency and mode shape for the simply supported rectangular plate can be expressed as follows (Szilard 1974):

$$\omega_{mn} = \pi^2\left[\frac{m^2}{L_x^2} + \frac{n^2}{L_y^2}\right]\sqrt{\frac{D}{\rho_{\mathrm{p}} t_{\mathrm{p}}}} \tag{9}$$

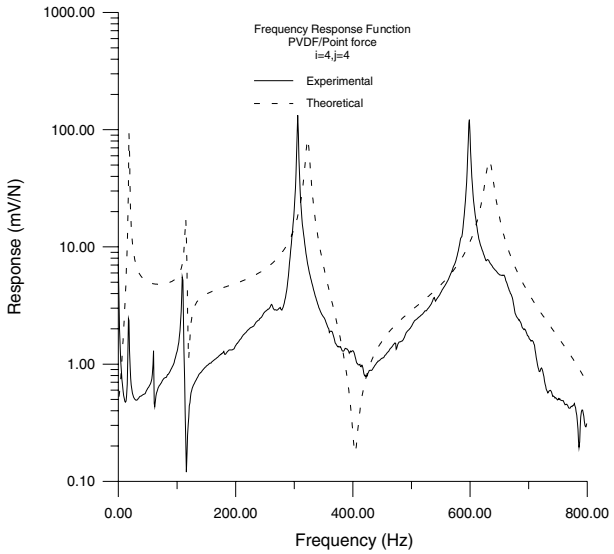

Figure 6. Frequency response function of the cantilever beam.

$$\phi_{mn}(x, y) = \phi_m(x)\phi_n(y) = \sin\alpha_m x \sin\alpha_n y \tag{10}$$

where

$$D = \frac{E_{\mathrm{p}} t_{\mathrm{p}}^3}{12(1-\nu_{\mathrm{p}}^2)} \tag{11}$$

$$\alpha_m = \frac{m\pi}{L_x}, \qquad \alpha_n = \frac{n\pi}{L_y}. \tag{12}$$

The FRF between the ith PVDF sensor and the jth point force actuator, as shown in figure 2, can be derived as follows:

$$\alpha_{v_i f_j}(\omega) = \frac{V_{v_i}}{F_j} = \sum_{n=1}^{\infty}\sum_{m=1}^{\infty} \frac{\phi_{mn,i}^{v}\phi_{mn,j}^{f}}{(\omega_{mn}^2 - \omega^2) + \mathrm{i}(2\xi_{mn}\omega_{mn}\omega)} \tag{13}$$

where

$$\phi_{mn,j}^{f} = \frac{1}{\sqrt{\rho_{\mathrm{p}} t_{\mathrm{p}}\left(\frac{L_x}{2}\frac{L_y}{2}\right)}}\phi_{mn}(x_{f_j}, y_{f_j}) \tag{14}$$

$$\phi_{mn,i}^{v} = \frac{\left[e_{31}\left(\frac{1}{\alpha_n^2}\right) + e_{32}\left(\frac{1}{\alpha_m^2}\right)\right]}{\sqrt{\rho_{\mathrm{p}} t_{\mathrm{p}}\left(\frac{L_x}{2}\frac{L_y}{2}\right)}} k_v[\phi_m'(x_{v_{2i}}) - \phi_m'(x_{v_{1i}})] \times [\phi_n'(y_{v_{2i}}) - \phi_n'(y_{v_{1i}})] \tag{15}$$

$$\phi_m'(x_{v_{2i}}) - \phi_m'(x_{v_{1i}}) = -2\alpha_m \sin\alpha_m \frac{l_{vx}}{2}\phi_m(x_{v_i}) \tag{16}$$

$$\phi_n'(y_{v_{2i}}) - \phi_n'(y_{v_{1i}}) = -2\alpha_n \sin\alpha_n \frac{l_{vy}}{2}\phi_n(y_{v_i}) \tag{17}$$

$$k_v = \frac{t_v}{\varepsilon A_v}\left(\frac{t_{\mathrm{p}} + t_v}{2}\right). \tag{18}$$

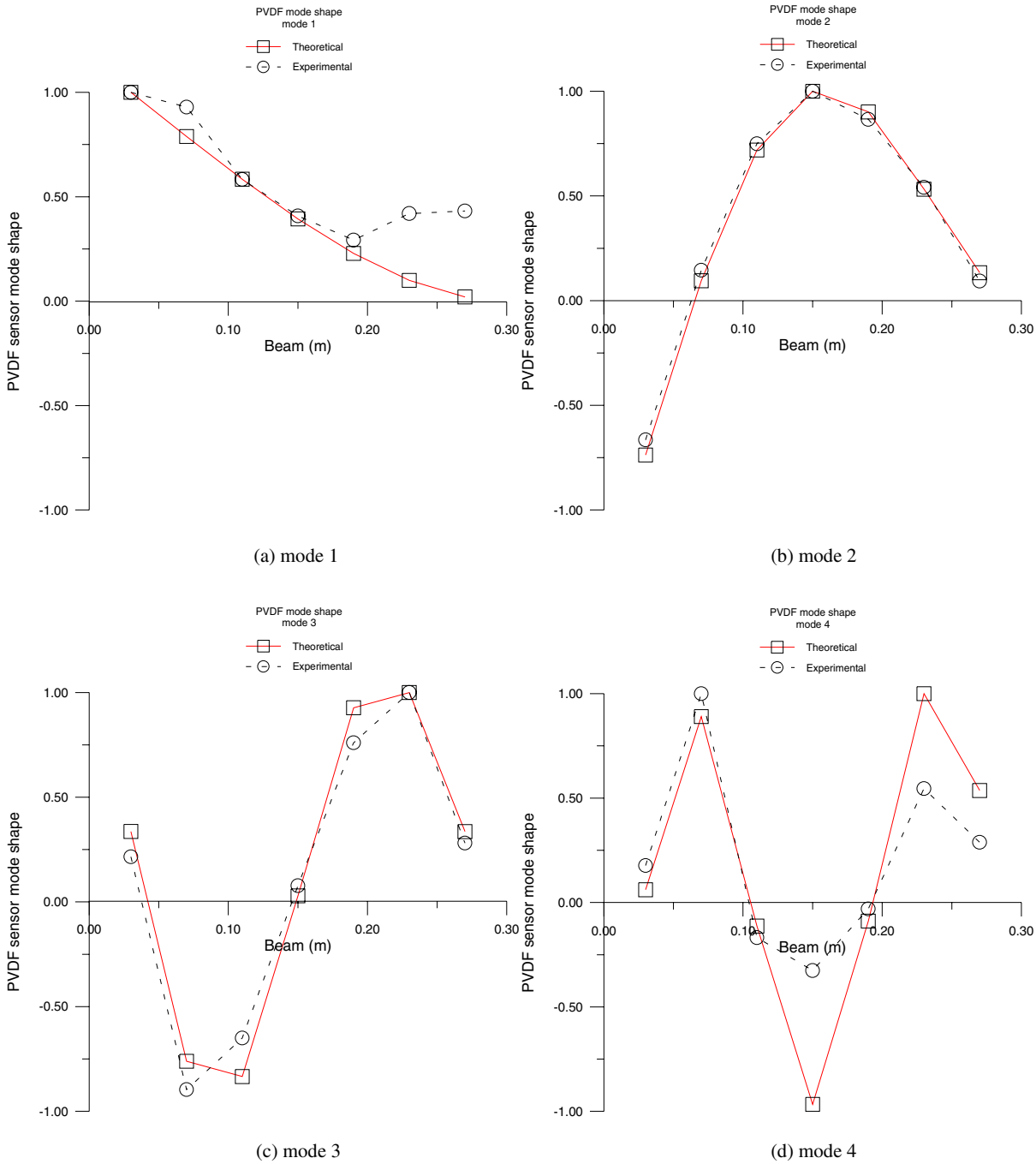

Figure 7. Theoretical and experimental PVDF sensor mode shape of the cantilever beam.

Table 5. MAC values between theoretical and experimentally predicted mode shapes of cantilever beam.

Mode	1	2	3	4
1	**0.4462**	0.0886	0.0874	0.0363
2	0.1243	**0.8214**	0.0323	0.0195
3	0.0609	0.0228	**0.9555**	0.0201
4	0.1846	0.0023	0.0015	**0.7851**

Table 6. Physical properties of simply supported plate.

Material	Steel
Length, L_x (m)	0.38
Width, L_y (m)	0.3
Thickness, t_p (m)	0.002
Density, ρ_p (kg m^{-3})	7870
Young's modulus, E_p (N m^{-2})	207×10^9
Poisson ratio, ν_p	0.292

In particular, the PVDF sensor mode shape functions as shown in equation (15) are the slope difference mode shapes. For simply supported boundary conditions, the slope difference mode shape can be shown to be proportional to the displacement mode shape as shown in equations (16) and (17).

Table 7. Comparison of the natural frequencies of the simply supported plate between theoretical and experimental results.

Natural frequency	Theoretical (Hz)	Experimental (Hz)		Error percentage (%)	
		Acc./hammer[a]	PVDF/hammer	Acc./hammer	PVDF/hammer
$f_{1,1}$	87.71	90.12	86.96	2.75	−0.86
$f_{2,1}$	188.74	189.96	185.91	0.64	−1.50
$f_{1,2}$	249.81	252.20	246.98	0.96	−1.13
$f_{2,2}$	350.85	341.23	335.98	−2.74	−4.24
$f_{3,1}$	357.13				

[a] Wang and Chen (1997).

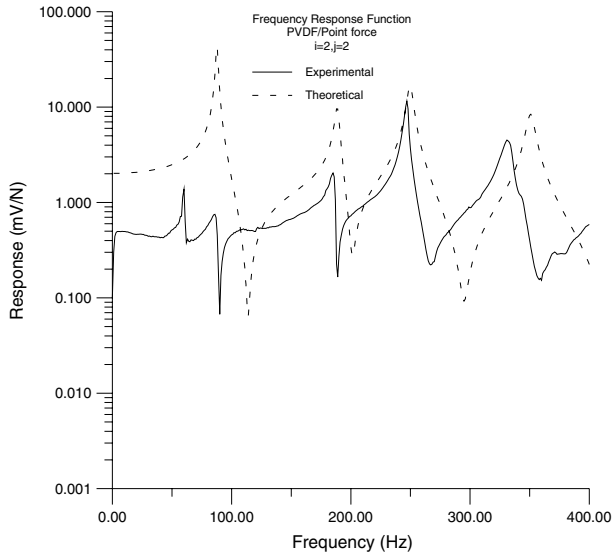

Figure 8. Frequency response function of the simply supported plate.

To perform experimental modal analysis, at least, either a row or a column of the FRF matrix must be measured. By roving the actuator, a row of the FRF matrix can be obtained; and by roving the sensor, a column of the FRF matrix will be obtained. In summary, when the sensor is roving with the actuator fixed during testing, a column of the FRF matrix can be determined. The extracted mode shape will then be characterized by the sensor mode shape. Conversely, when the actuator is roving with the sensor fixed, a row of the FRF matrix can be obtained. The extracted mode shape will then be characterized by the actuator mode shape (Wang 1998). In this work, the hammer actuator is fixed, and the PVDF sensor is roving; therefore, a column of the FRF matrix can be obtained. The extracted mode shapes will then be the PVDF sensor mode shapes.

3. Experimental set-up and procedures

The objective of experimental modal analysis is to obtain the first four modes. The grid of the cantilever beam is shown in figure 3(a) and numbered up to seven locations. The point force is located at position 2. The simply supported plate is shown in figure 4(a) and numbered up to 25 locations. The hammer actuator is applied at position 2, while the PVDF sensors are evenly distributed in every position. The cantilever beam and simply supported plate substance pictures are shown in figures 3(b) and 4(b), respectively. The test equipment layout

Table 8. The experimental modal damping of the simply supported plate.

Mode	Damping ratio (%)
$\xi_{1,1}$	2.40
$\xi_{2,1}$	0.75
$\xi_{1,2}$	0.61
$\xi_{2,2}$	0.93

Table 9. MAC values between theoretical and experimentally predicted mode shapes of simply supported plate.

Mode	(1, 1)	(2, 1)	(1, 2)	(2, 2)
(1, 1)	**0.986 2**	0.000 01	0.000 005	0.000 002
(2, 1)	0.002	**0.943**	0.001 85	0.000 8
(1, 2)	0.000 07	0.000 3	**0.958 6**	0.000 03
(2, 2)	0.000 8	0.016 1	0.011 5	**0.895 5**

for the simply supported plate is depicted in figure 5. The hammer actuator is applied to excite the structure and input to channel A. The structure response is measured by the PVDF sensor and input to channel B. The dual-channel FFT analyzer (BK3550) captures both the input force of the hammer actuator and the output voltage of the PVDF sensor, respectively, and calculates the frequency response function. Let the hammer actuator be fixed and the PVDF sensors roving; a column of the FRFs can be measured and transported to CADA-PC through the IEEE-488 interface. The general purpose curve fitting software, CADA-PC, is used to extract the system modal parameters. Natural frequencies, modal damping ratios and PVDF mode shape functions of the structure can be extracted.

4. Results and discussion

In the following discussion, the theoretical and measured FRFs are compared. The modal parameters determined from the modal parameter extraction process will also be evaluated.

4.1. Results and discussion for cantilever beam

The physical properties of the cantilever beam and PVDF sensor are shown in tables 1 and 2. The theoretical natural frequencies and mode shapes can be determined from theoretical analysis. By assuming the modal damping ratios to be 0.01, one can obtain the theoretical FRF.

4.1.1. Verification of frequency response functions. Figure 6 shows the typical point FRF for $i = 4$, $j = 4$ where the

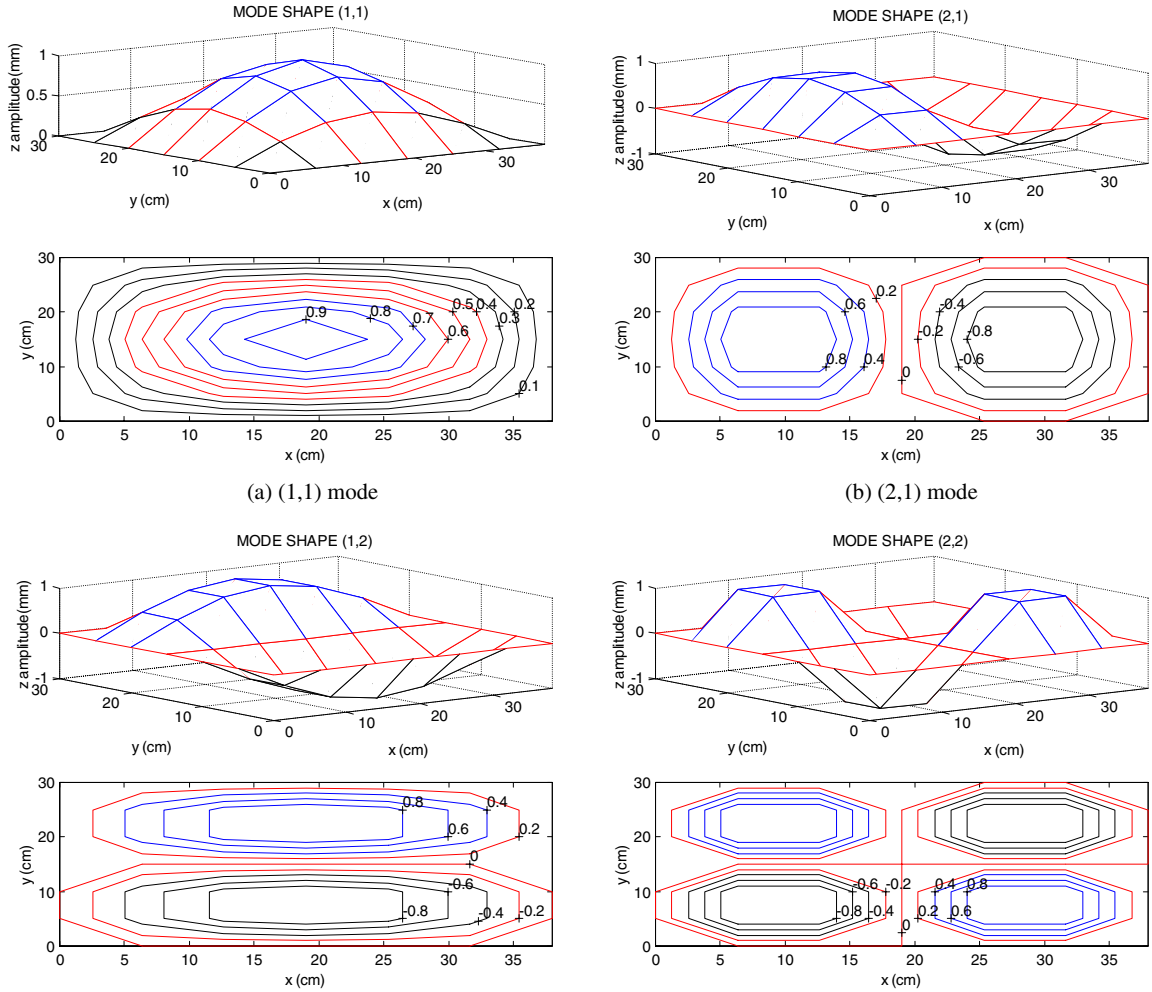

(a) (1,1) mode (b) (2,1) mode

(c) (1,1) mode (d) (2,1) mode

Figure 9. Theoretical PVDF sensor mode shape of simply supported plate.

sensing point is the same as the actuation one. There are antiresonance points between resonances. In figure 6, the solid line denotes the experimental FRF; the dashed line denotes the theoretical FRF. The FRF curves generally agree between theoretical and experimental ones. The amplitude in the low frequency range of the theoretical and experimental FRFs is somewhat different. This may be due to the PVDF sensors contributing to increase the structural damping effect. There is a peak at 60 Hz due to the electronic noise. In summary, the measured FRFs are applicable to further operation of the extraction of modal parameters.

4.1.2. Verification of modal parameters. Table 3 shows the comparison of natural frequencies between the theoretical and experimental results for the first four modes. The natural frequencies obtained from the PVDF sensors are within -5.93% differences. On the other hand, the natural frequencies obtained from the accelerometer sensor are within -2.18%. The gradual shift of natural frequencies could be the cause of the mass effect of PVDF sensors and can be easily adjusted.

In theoretical analysis, the structural damping ratios cannot be obtained and so henceforth can be assumed to be 0.01 to generate the FRFs. The modal damping ratios were extracted through the curve-fitting process and are shown in table 4. The first modal damping ratio is 4.95% higher than the expected damping ratio 0.5–1.0% for steel material (Harris and Crede 1976). This may be due to the PVDF sensors contributing to increase the structural damping effect. Nevertheless, the extracted modal damping ratios generally agree with steel materials.

This work is to determine the modal parameters of the first four modes of interest. It should be noted that the fixed hammer actuator and the roving PVDF sensors are adopted to perform the FRF measurement. Therefore, the PVDF mode shape function can be extracted through the curve-fitting process. Both the experimental and theoretical mode shapes that are the slope difference between the two edges of the PVDF sensors are shown in figures 7(a)–(d). One can observe that both mode shapes agree reasonably well. The PVDF slope sensor mode shapes appear as the mirror image of the displacement mode shape against the clamped end (Wang and Wang 1997). To further examine the correctness of the extracted mode shapes, the MAC (modal assurance criterion) (Ewins 1986, Heylen and Janter 1990) is the indicator for the evaluation of similarity between two mode shapes. Table 5 shows the

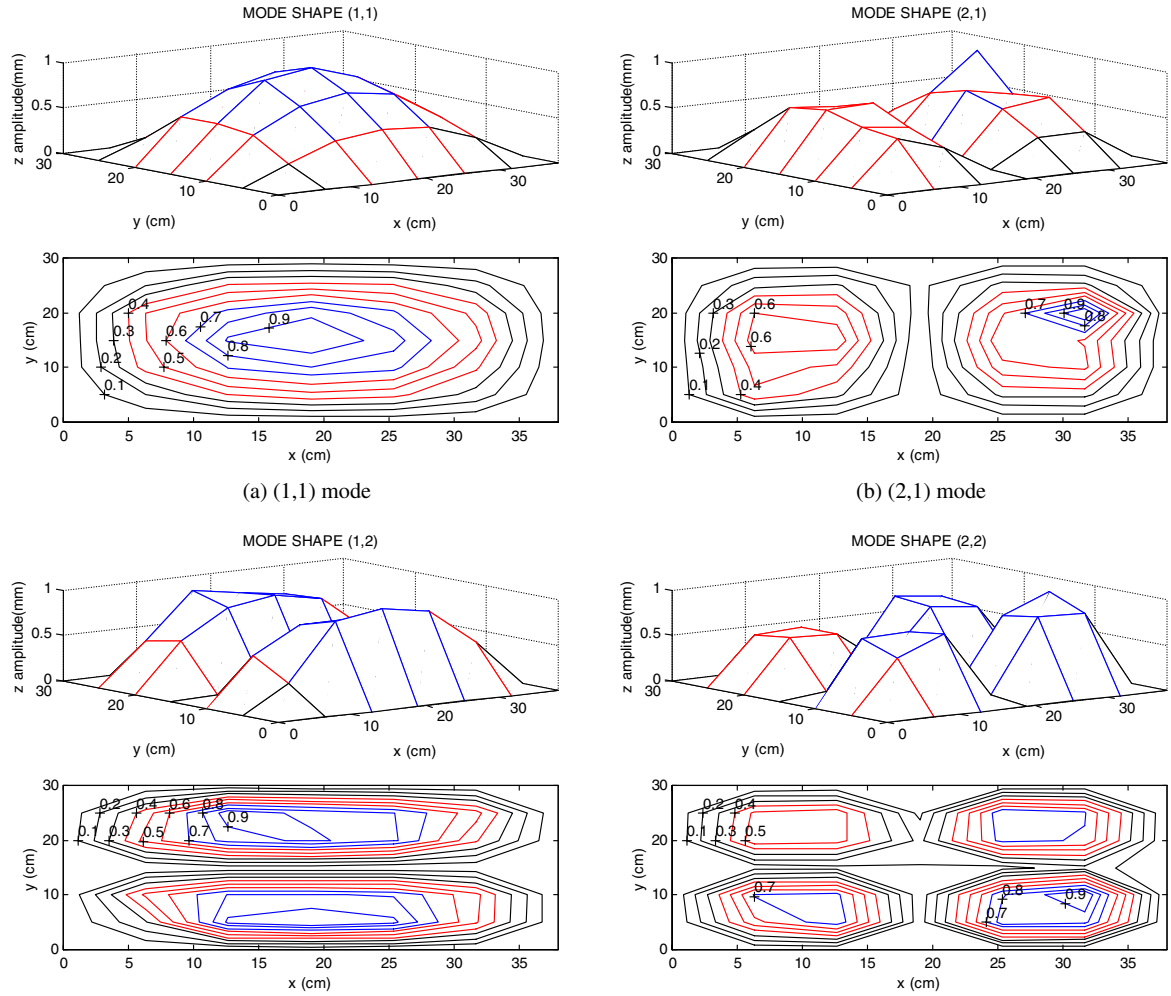

(a) (1,1) mode

(b) (2,1) mode

(c) (1,2) mode

(d) (2,2) mode

Figure 10. Experimental PVDF sensor mode shape of simply supported plate.

MAC matrix for comparison between the experimental and theoretical mode shapes. That the diagonal terms of the MAC matrix approach one represents the perfect agreement between the two mode shapes. When the off-diagonal terms of the MAC matrix are close to zero, the two mode shapes possess perfect orthogonality. One can observe that both experimental and theoretical mode shapes have a certain degree of similarity and possess orthogonality of the mode shapes, except MAC(1, 1) = 0.4462. This is the reason that two points near the free end appear relatively in high value as seen from figure 7(a).

4.2. Results and discussion for simply supported plate

The physical properties of the simply supported plate are shown in table 6. The following will show the verification of the FRF and modal parameters, respectively.

4.2.1. Verification of frequency response functions. Figure 8 shows the FRFs for $i = 2$, $j = 2$. The 60 Hz electrical noise peak also appears in the experimental FRF. The amplitude in the low frequency range of the theoretical FRF is slightly different from the experimental ones. The resonance frequencies and the shape of the FRFs show reasonable agreement between the theoretical and experimental FRFs. Generally speaking, in spite of the 60 Hz electric noise the measurement of FRFs is satisfactory and suitable for a further curve fitting process to extract modal parameters of the simply supported plate.

4.2.2. Verification of modal parameters. Table 7 shows the comparison of natural frequencies between the theoretical and experimental results for the first four modes. Except for the natural frequency of mode (2, 2), having −4.24% difference, the others are within −1.5% difference. The natural frequency of mode (2, 2) may be affected by the (3, 1) mode. The natural frequency of mode (3, 1) is 357.13 Hz near mode (2, 2), 350.85 Hz. The test plate is well simulated for the simply supported boundary conditions (Wang and Chen 1997). The natural frequencies obtained from conventional modal testing are also shown in table 7. The PVDF film transducers work well in predicting the natural frequencies of the structure.

The modal damping ratios extracted from the curve fitting process for the first four modes are also listed in table 8. $\xi_{1,1}$ is 2.4% higher than the expected damping ratio 0.5–1.0% for steel material. Other modal damping ratios agree well. However, it

should be noted that the adhesion and material effect of PVDF films can also contribute to increase damping but is neglected in theoretical analysis.

The first four theoretical displacement mode shapes of the simply supported plate are depicted in figure 9, and the experimental PVDF sensor mode shapes are shown in figure 10. In figure 10, the mode shapes are depicted in amplitude, so all values are positive. One can observe that there are certain degrees of similarity between figures 9 and 10. The PVDF sensor mode shapes as shown previously are proportional to the displacement mode shapes and are validated in figure 10. The use of PVDF sensors for the experimental modal testing is demonstrated and shown to be promising.

MACs between the theoretical and experimentally predicted mode shapes are tabulated in table 9. One can see that the diagonal terms close to one indicate the agreement between the theoretical and experimental mode shapes. The off-diagonal terms near zero indicate the orthogonality of the mode shapes. In summary, the use of PVDF sensors does successfully perform experimental modal testing of the simply supported plate. The modal parameters, including natural frequencies, modal damping ratios and PVDF sensor mode shapes, are obtained and physically interpreted. The modal information is useful for further applications in structural fault diagnosis as well as other applications such as structural vibration and acoustic control.

5. Conclusions

This paper experimentally verifies the use of PVDF sensors for cantilever beam and simply supported plate modal testing. The system modal parameters, including natural frequencies, damping ratios and mode shapes, are properly identified. In particular, the extracted mode shapes are physically interpreted as the slope difference between two edges of the PVDF sensors. The FRFs of PVDF sensors can also be derived and expressed in conventional modal format. The conventional modal parameter extraction methods may be suitable to apply to determine the modal parameters for the PVDF film structures. The system information is properly provided and can be adopted for control application. The idea of smart structure testing (SST) is experimentally validated.

Acknowledgments

The authors gratefully thank the National Science Council of Taiwan for partial support for this work under contract number NSC92-2212-E-020-006.

References

Blevins R D 1979 *Formulas for Natural Frequency and Mode Shape* (New York: Van Nostrand-Reinhold)

Collet M and Jezequel L 1994 A new approach to modal filtering with laminated piezo-electric sensors *Proc. 12th Int. Conf. on Modal Analysis* pp 246–54

Collins S A, Padilla C E, Notestine R J, von Flotow A H, Schmitz E and Ramey M 1992 Design, manufacture, and application to space robotics of distributed piezoelectric film sensors *J. Guid. Control* **15** 396–403

Ewins D J 1986 *Modal Testing: Theory and Practice* (Letchworth: Research Studies Press LTD)

Galea S C, Chiu W K and Paul J J 1993 Use of piezoelectric films in detecting and monitoring damage in composites *J. Intell. Mater. Syst. Struct.* **4** 330–6

Han S and McConnell K G 1991 Analysis of frequency response functions affected by the coupled modes of the structure *Int. J. Anal. Exp. Modal Anal.* **6** 147–59

Harris C M and Crede C E 1976 *Shock and Vibration Handbook* (New York: McGraw-Hill)

Heylen W and Janter T 1990 Extensions of the modal assurance criterion *Trans. ASME* **112** 468–72

Hu X and McConnell F G 1993 Stinger mass compensation part two: experimental investigation *Int. J. Anal. Exp. Modal Anal.* **8** 45–54

Hubbard J E 1987 Distributed sensors and actuators for vibration control in elastic components *Noise-Con 87* pp 407–12

Lee C K and Moon F C 1990 Modal sensors/actuators *J. Appl. Mech.* **57** 434–41

Meirovich L 1986 *Elements of Vibration Analysis* (New York: McGraw-Hill)

Norwood C 1995 The measurement of natural frequencies and mode shapes of submerged cylinders using PVDF strip excitation *Proc. Inter-Noise 95* pp 1337–40

Sun F P, Liang C and Rogers C A 1994 Experimental modal testing using piezoceramic patches as collocated sensor-actuators *Proc. 1994 Conf. on SEM Spring and Exhibits* pp 871–9

Szilard R 1974 *Theory and Analysis of Plates Classical and Numerical Methods* (Englewood Cliffs, NJ: Prentice-Hall)

Tanaka N, Snyder S D and Hansen C H 1996 Distributed parameter modal filtering using smart sensors *Trans. ASME J. Vib. Acoust.* **118** 630–40

Wang B T 1996 Characterization of transfer functions for piezoceramic and conventional transducers *J. Intell. Mater. Syst. Struct.* **7** 390–8

Wang B T 1998 Structural modal testing with various actuators and sensors *Mech. Syst. Signal Process.* **12** 627–39

Wang B T and Chen R L 1997 Experimental modal analysis of a simply supported plate *Bull. Natl Pingtung Univ. Sci. Technol.* **6** 273–81 (in Chinese)

Wang B T and Wang C C 1997 Feasibility analysis of using piezoceramic transducers for cantilever beam modal testing *Smart Mater. Struct.* **6** 1–11

Worden K, Wright J R, Al-Hadid M A and Mohammdd K S 1994 Experimental identification of multi degree-of-freedom nonlinear systems using restoring force methods *Int. J. Anal. Exp. Modal Anal.* **9** 35–55